AIAA 80-1804R

Experimental Investigation of a Wing with Controlled Midspan Flow Separation

V.F. Meznarsic* and L.W. Gross*
McDonnell Douglas Corporation, St. Louis, Mo.

A wing with a bounded region of separated flow at high angles of attack was tested in the McDonnell Aircraft Company low-speed wind tunnel. The model configuration was chosen to provide a test case for the development of an analytical method for the calculation of the flow about stalled wings. Extensive data were obtained on wing surface pressure, the boundaries of the separated flow bubble above and aft of the wing, and flow visualization. Flowfield velocity measurements were integrated to determine the displacement thicknesses of the viscous flow, which were subsequently used to determine an equivalent inviscid shape. The equivalency was verified by comparing the calculated potential flow pressures of this shape with the measured pressures.

Introduction

FAVORABLE aerodynamic characteristics in the stalled flight regime are becoming increasingly important to modern fighter aircraft as flight envelopes are expanded to exploit the high-angle-of-attack combat environment. This requires a capability to design departure resistance into fighter aircraft in the early stages of development. Recent evidence for unswept wings suggests that controlled midspan separation, in concert with attached inboard and outboard flow, may significantly improve departure characteristics by softening the abrupt stall associated with other separation patterns.[1,2] It is not obvious at this time that this type of controlled stall progression is the best design approach for increased departure resistance for fighter aircraft. However, it is desirable to determine analytically the stalling characteristics of fighter wings in order to supplement developmental wind-tunnel testing. To do this, it is necessary to predict the conditions under which flow separation will occur, regardless of the type of flow separation. In addition, it is necessary to predict the loads on the wings and control surfaces when there are regions of separated flow present.

Analytical techniques are being developed at McDonnell Aircraft Company to model regions of flow separation and to predict the aerodynamic forces under these conditions.[3] To support this effort, it was necessary to provide experimental data for the description of the flow within the separation bubble and additional wing flowfield data. On the basis of a preliminary analysis, the required data were determined to be: 1) extensive surface pressure measurements to provide estimates of spanwise pressure gradients, 2) measurements of the boundaries of the separated flow bubble above and aft of the stalled wing, 3) an estimate of the shed vorticity, and 4) flow visualization data to identify regions of flow into and out of the bubble. A review of the pertinent experimental data indicated that no data were available that satisfied all of these requirements. Therefore, an experimental program was initiated, under MCAIR Independent Research and Development funding, to supply the necessary measurements.[4] This paper discusses the results of this experimental effort.

Presented as Paper 80-1804 at the AIAA Aircraft Systems and Technology Meeting, Anaheim, Calif., Aug. 4-6, 1980; submitted Sept. 10, 1980; revision received Aug. 31, 1981.

*Technical Specialist, Technology—Aerodynamics, McDonnell Aircraft Company.

Test Setup

The wind-tunnel model tested was originally built for an investigation of wing and jet interactions.[5] It is an unswept, constant chord, symmetrical wing with an aspect ratio of 4.0 and a NACA 0012 airfoil section. It was felt that the separated region should be bounded on both sides by attached flow so that an isolated separation bubble could be investigated. The configuration was not intended to be representative of those being developed for improved airplane departure characteristics. Several methods for providing a controlled region of separated flow were evaluated, including trailing-edge flaps, leading-edge slats, and drooped leading edges. It was established that the use of leading-edge slats would yield the best definition of the separation region with the least loss of pressure data due to modification of the model. The selected model configuration is shown in Fig. 1. Two sets of outboard slats were provided in order to vary the width of the separated region. The distance between the inboard and outboard slat segments is termed the slat "spacing." The slats also had two vertical positions with respect to the wing: high and low. After measurement of the wing pressure distributions with the four resulting slat/wing configurations, flowfield measurements were taken only for the configuration with the low slat position and narrow region of separated flow.

The basic wing model has 352 pressure taps on its surface, arranged as 22 pressure taps at each of 16 spanwise stations. The pressure taps at each spanwise station include 10 on the upper and lower surfaces, one on the leading edge and one on the trailing edge. Pressures were not measured on the slats. A cross section of the wing and slat showing the spanwise and chordwise locations of the pressure taps on the wing is included in Fig. 1.

Figure 2 is a schematic of the model as it was mounted in the advanced design wind tunnel at McDonnell Aircraft Company. Flowfield surveys over and aft of the model were made by a wake survey rake as indicated in the figure. The rake consists of five pairs of total pressure and static pressure tubes. The tubes are 1/2 in. apart to preclude mutual interference and the tube pairs are spaced 1 in. apart. For this test the total and static pressure tubes were in the same horizontal plane. The rake was translated horizontally and vertically while the wind tunnel was running. The rake was translated horizontally in the chordwise direction when the tunnel was off. This allowed the full spatial volume behind and above the wing to be mapped. The drawbacks of pitot-static measurements in a separated flowfield were recognized. However, a detailed knowledge of the velocity vector field

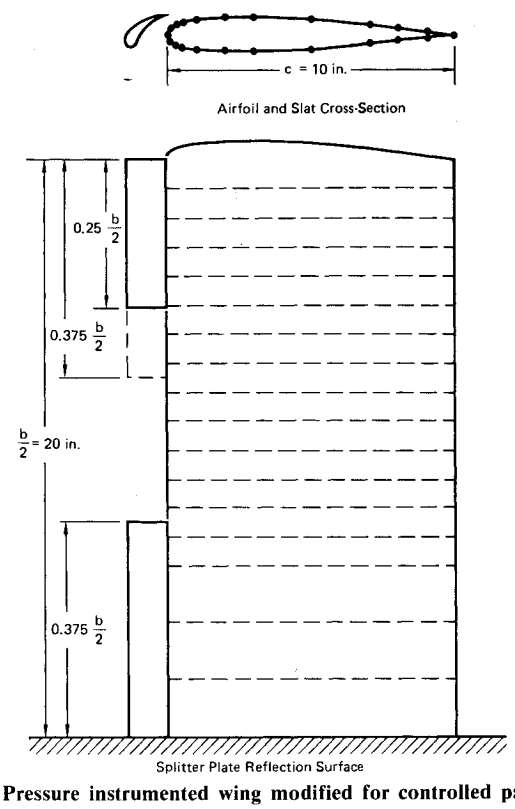

Fig. 1 Pressure instrumented wing modified for controlled partial span stall test.

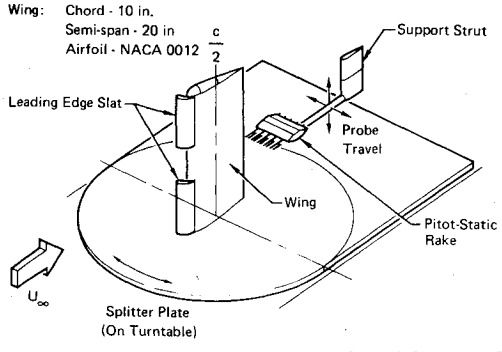

Fig. 2 Experimental test setup for controlled partial span stall test.

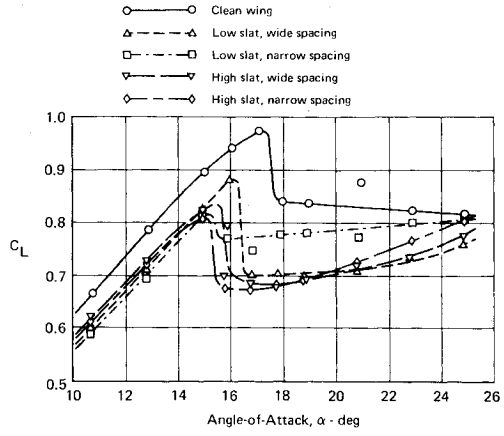

Fig. 3 Lift curves for controlled separation wing (slat lift not included).

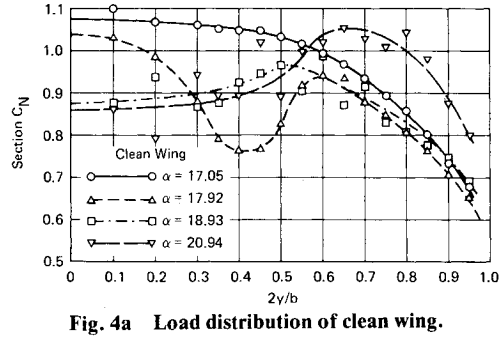

Fig. 4a Load distribution of clean wing.

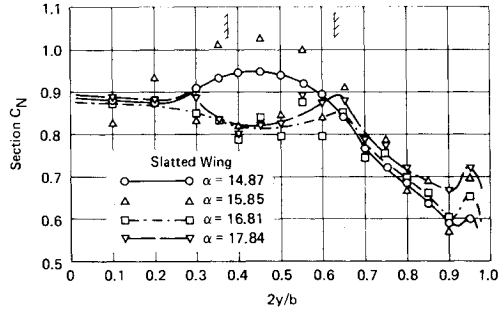

Fig. 4b Load distribution of controlled separation wing (slat load not included).

was not required, and the velocities as measured were felt to be adequate for the calculation of the displacement thickness of the separated flow.

Flow visualization studies were conducted after covering the model surface with paper. The paper was coated so that it would be impervious to the lampblack suspended in Coolanol used for the studies. A thin layer of this mixture was spread on the model. With the wind on, the mixture was distributed over the surface of the model by the surface airflow. A record of this flow pattern remained after the Coolanol evaporated.

Test Results

The spanwise distribution of normal force and the total wing normal force were determined by integration of the surface pressures. It should be noted that this does not include the normal force contribution of the slats which were not instrumented. The variation of total wing lift coefficient with angle of attack is shown in Fig. 3 for the unslatted wing and the four slat configurations tested. The early stall of the slatted wings is due to the actions of the slat tip vortices on the unprotected part of the wing. The vortices from the outboard tip of the inner slat segment and the inboard tip of the outer segment both induce an upwash at the midsemispan of the wing. This additional local angle of attack causes early separation over a sufficiently large portion of the wing that the total lift drops.

Figure 4 shows the spanwise load distributions on the wing at angles of attack just before and just after the stall. The load distribution for the unslatted or clean wing is shown as Fig. 4a, and the load distribution for the slatted configuration for which the flowfield data were measured is shown as Fig. 4b. It can be seen that the inboard portion of the clean wing stalls first, as expected. After the inboard section stalls, the normal force in this region stays relatively constant, and the boundary of the stalled area moves outboard with increasing angle of attack.

At the angle of attack just at the stall ($\alpha = 17.9$ deg), it appears that the clean wing stalled near the midspan (Fig. 4a). However, inspection of the chordwise pressure distributions at this angle of attack showed that the separation bubble extended over almost all of the inboard region. The additional lift inboard of $2y/b = 0.25$ comes from a narrow strip of attached flow near the wing leading edge. Apparently there is a spanwise variation in the rate at which separation moves

forward with increasing angle of attack, probably due to slight variations of the shape of the model.

Of the slatted wing configurations, that with the low slat position and narrow spacing was judged to give the best example of bounded separation. The high slat position did not delay separation on the protected parts of the wing to very high angles of attack, while the configuration with the low slat and wide spacing did not isolate the separated flow from the wing tip vortex. All of the flowfield data within the separation bubble was taken with the chosen configuration at an angle of attack $\alpha = 16.81$ deg.

The spanwise load distributions of the slatted wing (Fig. 4b) show that the slats worked as desired. In the regions protected by the slats, there was little normal force loss at the stall, and these regions continued to add normal force as the angle of attack increased. In the unprotected region, the normal force loss at stall was large, and there was little or no normal force increase as angle of attack was increased. The chordwise pressure distributions for this configuration at the angle of attack at which the flowfield data were taken ($\alpha = 16.81$ deg) are shown in Fig. 5.

It is well known that airfoil or wing stall causes the noise and vibration levels in a wind tunnel to rise dramatically. The reason is illustrated by the normal force and pressure data shown in Figs. 4 and 5. These figures show a large spanwise scatter of the data at angles of attack beyond the stall. The nature of this data scatter is further illustrated by plotting the spanwise variation of the pressure coefficients of Fig. 5 at several chordwise stations. This is shown in Fig. 6. It can be seen that if the loads or pressures at alternating spanwise stations were drawn on separate graphs, each graph would show a consistent trend, but the two graphs would be different. This can be explained by noting that eight Scanivalves each measured the pressures at two adjacent spanwise stations sequentially for the total of 16 spanwise stations. Therefore, the pressures at alternating spanwise stations were measured at the same time. The consistency of the chordwise pressure distributions for alternating rows (Fig. 5) suggest that the flow switched from one separation state to another rather than pulsing in a random fashion. This could be verified using conditional sampling techniques. In the meantime the pressure distributions corresponding to the state of greatest

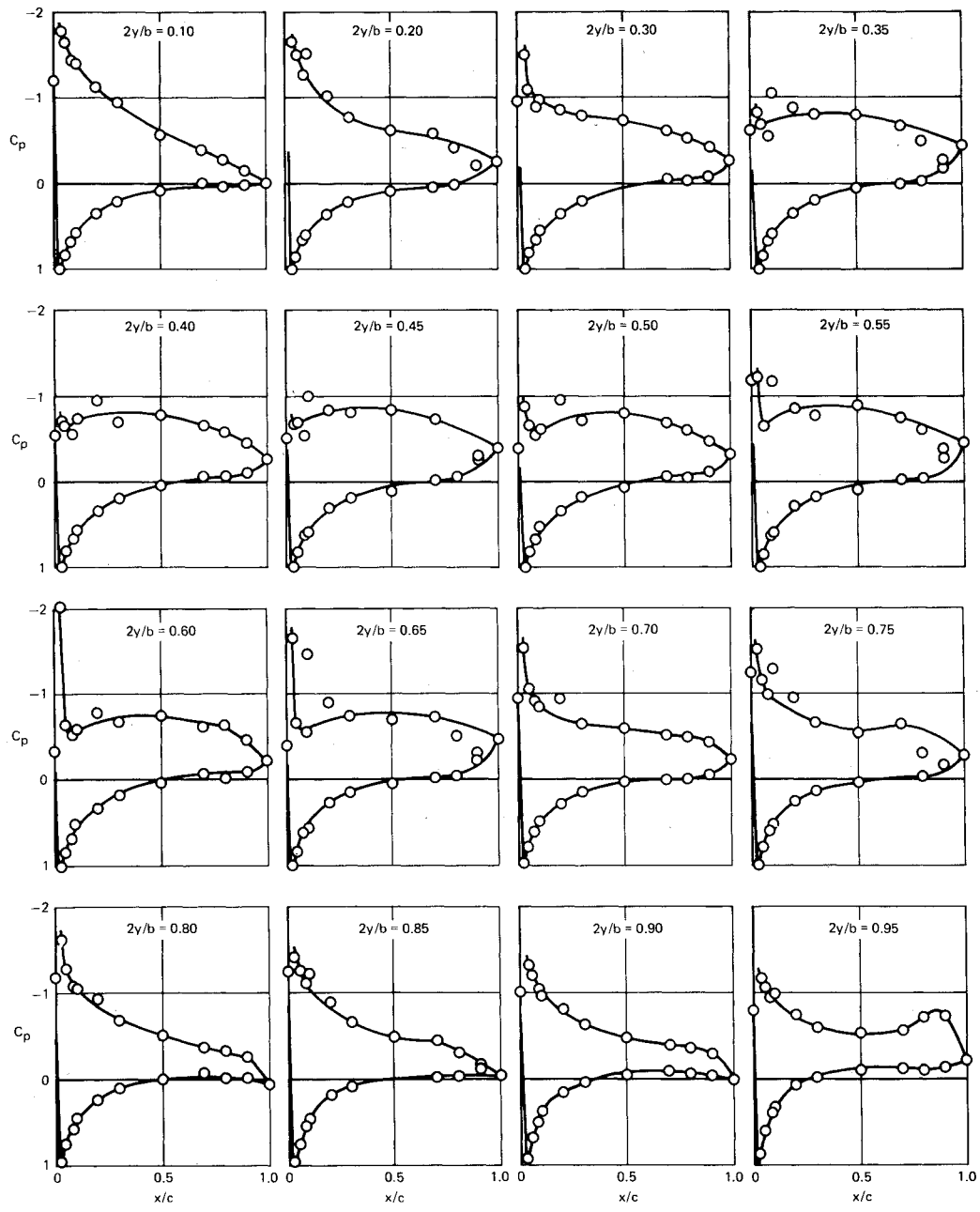

Fig. 5 Chordwise pressure distributions for controlled separation wing ($\alpha = 16.8$ deg, $R_c = 1.1 \times 10^6$).

flow separation were used for the subsequent analysis. These pressure distributions are characterized by higher pressures forward of $x/c=0.5$ due to loss of the leading-edge pressure peak, and lower pressures aft of this point induced by a larger separation bubble.

Figures 7-10 illustrate the changes of the wing surface flow associated with a shift from attached to separated flow. At a corrected angle of attack of 14.96 deg (14 deg geometric setting), the clean (unslatted) wing is on the verge of stall. The flow is attached to the surface everywhere except over a small portion of the trailing edge near the splitter plate wall. Increasing the angle of attack to 16.2 deg caused flow separation to move all the way to the leading edge over a portion of the wing (Fig. 8).

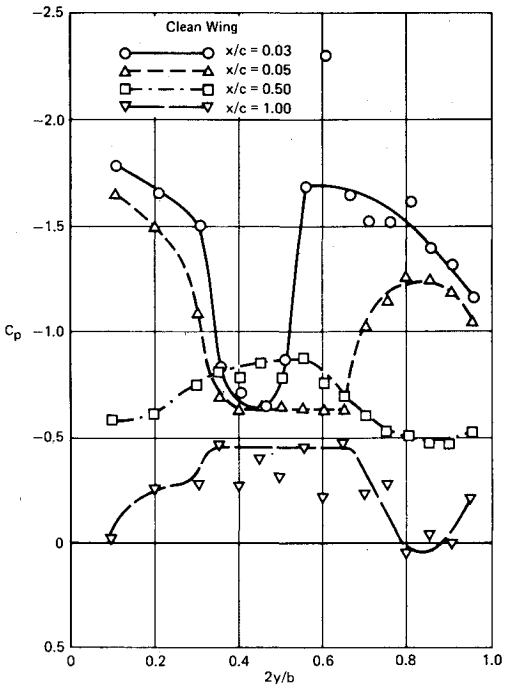

Fig. 6 Spanwise variation of pressure coefficient at given chord positions (controlled separation wing, $\alpha=16.8$ deg, $R_c=1.1\times10^6$).

The circulatory surface pattern of Fig. 8 is characteristic of three-dimensional separated flows, and similar patterns are reported in Refs. 6-9. Due to the downwash generated by the wing tip vortex the flow near the wing tip remains attached after the inboard portion of the wing has separated. Since the pressures near the leading edge of the attached flow region are lower than the pressures near the leading edge of the separated flow region, a secondary flow is induced on the wing surface that moves from the separated region to the attached flow region. Near the trailing edge, the lower pressures in the separated flow region cause the secondary flow to move from the attached flow into the separation bubble. The result is the large circulatory pattern shown in Fig. 8.

The slats of the controlled separation wing induce an upwash in the region between the slats. This increased local angle of attack causes the boundary layer to separate from the wing surface in this region at an angle of attack that is lower than that at which separation is observed on the clean wing. Figure 9 shows the surface flow patterns on the controlled separation wing at an angle of attack $\alpha=14.9$ deg. A similar pattern, closer to the trailing edge, was observed at $\alpha=13.9$ deg. In Fig. 9, separation occurred near the 20% chord station. The return flow divided itself into two circulatory patterns at both boundaries. The forward circulatory flow was the more energetic and extended from 20 to 40% chord. The outboard of these smaller circulatory flows was as energetic as the inboard, but picked up less of the lampblack-Coolanol mixture, probably due to the effects of gravity. It is interesting to note that the pattern between 20-40% chord is very similar to that observed for separation between the sidewalls of a wind tunnel.[6-8]

Once separation has moved to a point near the wing leading edge (Fig. 10), the near symmetry of the circulatory patterns becomes more obvious. The centerline of the separated flow does not coincide with the centerline of the gap between the

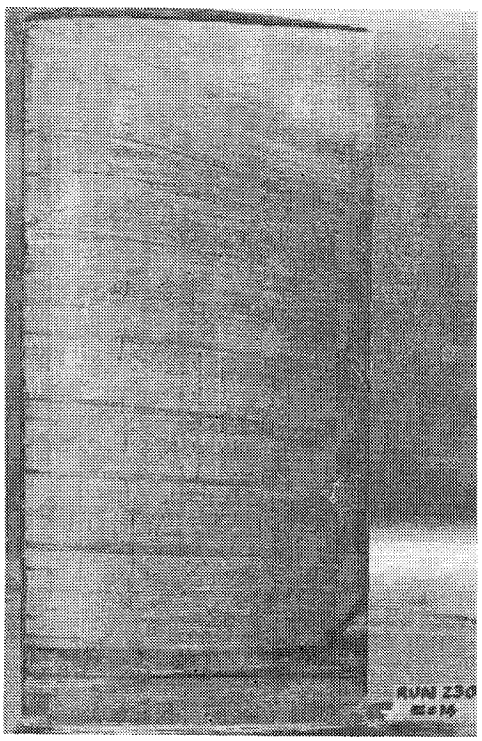

Fig. 7 Surface flow pattern of wing on verge of stall ($\alpha=15$ deg, $R_c=1.1\times10^6$).

Fig. 8 Surface flow pattern of stalled wing ($\alpha=16.2$ deg, $R_c=1.1\times10^6$).

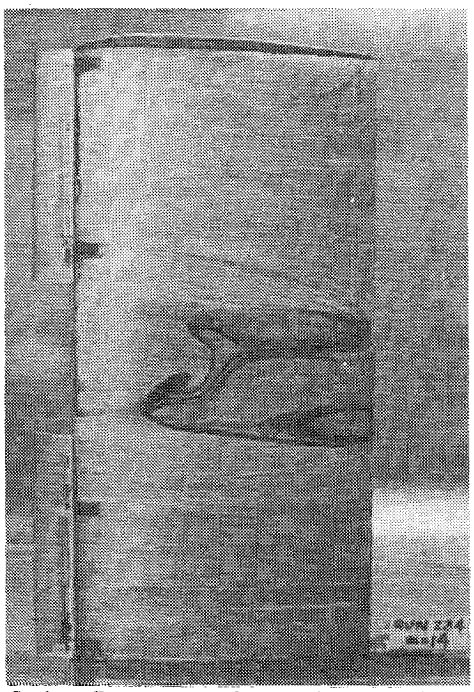

Fig. 9 Surface flow pattern of controlled separation wing with trailing-edge separation ($\alpha = 15$ deg, $R_c = 1.1 \times 10^6$).

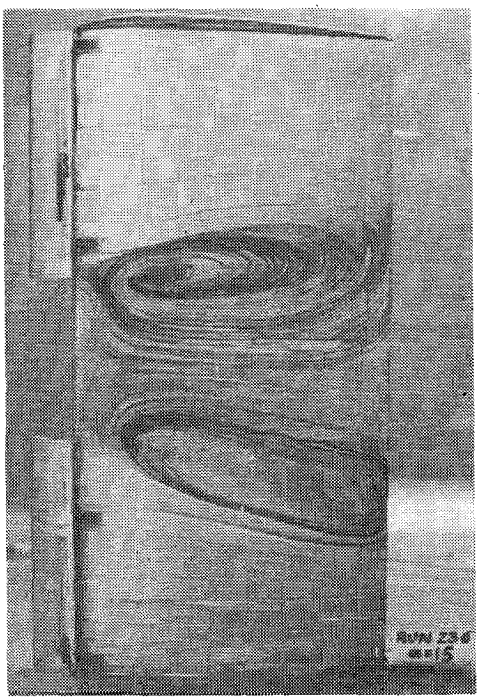

Fig. 10 Surface flow pattern of stalled controlled separation wing ($\alpha = 16.8$ deg, $R_c = 1.1 \times 10^6$).

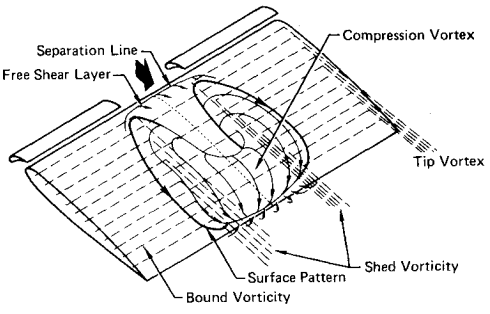

Fig. 11 Tentative flowfield model for controlled separation wing.

slats. Instead, it is displaced toward the wing root; it is inclined toward the wing root as well. Comparing these patterns with the load distribution shown in Fig. 4b shows that the boundaries of the separated region as defined by the load distribution coincides with the outer boundaries of the large circulatory patterns. Increases of angle of attack cause the separated flow region to widen. The centroid of the circulatory pattern also moves aft.

Analysis

An explanation of the relationship of these large circulatory surface patterns with other known features of the separated flowfield is proposed in Fig. 11. From two-dimensional separated flows, it is known that the separation bubble consists of a free shear layer above a relatively constant pressure reverse flow region. The bubble culminates with a compression vortex that compresses the flow from the bubble pressure to ambient pressure and turns a portion of the free shear layer flow into the reverse flow region. This compression vortex is fed by the shed vorticity due to the spanwise load gradients between the attached and separated flows. Thus, the large circulatory surface patterns are the visible terminations of the separated flow compression vortex. The vorticity that is shed into the flow via the wake is the net vorticity due to the differences of load across the region of separated flow. A similar separation bubble model has been described by Winkelmann.[9]

The static and total pressures measured above the wing and in the separated wake were used to determine the velocities in the wake. The static pressures were also used with the freestream total pressure to compute a Bernoulli velocity representative of the velocity that would have been present in the absence of viscosity. The difference between these velocities is assumed to be proportional to the local mass deficit due to viscosity, which appears to the potential flow as an equivalent solid body. This parallels the concept of the boundary-layer displacement thickness and the equivalent airfoil or body shapes used to simulate separated flow regions analytically in Ref. 3. Typical wake velocity profiles are shown in Fig. 12.

The displacement surfaces calculated from the wake velocity measurements are shown in Fig. 13. Behind those areas protected by the slats, the flow is attached to the surface and the wake is thin. Behind the unprotected surfaces, the flow is separated and the wake is thick. Spanwise sections of the displacement surfaces were also drawn and then developed into the isometric projection shown in Fig. 14. This is the wing shape that has an inviscid flowfield equivalent to the viscous, separated flow around the actual wing.

In order to determine that the shape of Fig. 14 is, indeed, equivalent to the separated flow, the shape was input into a potential flow calculation method. The potential flow method that was used is that of Woodward[10] as modified by Bristow.[11] Woodward simulates a wing or body by distributing mathematical singularities along a panelled reference plane. Then, the known boundary conditions on the surface of the aerodynamic shape are approximately satisfied on the reference plane. Bristow developed a version of this method in which the boundary condition for each singularity can be interchanged between the surface slope and the tangential flow velocity at the panel control point. This generalized boundary condition method allows the geometry to be specified where the equivalent wing shape is known, and a condition of no load to be specified across the wake behind the regions of attached flow.

Representative calculated pressures on the surface of the equivalent wing shape are compared to measured pressures in Fig. 15. The pressures measured on the surface of the wing are shown back to the wing trailing edge. Aft of the trailing edge, an average wake static pressure measured by the flowfield survey is shown. The representative chordwise pressure distributions are from the inboard attached flow region (Fig.

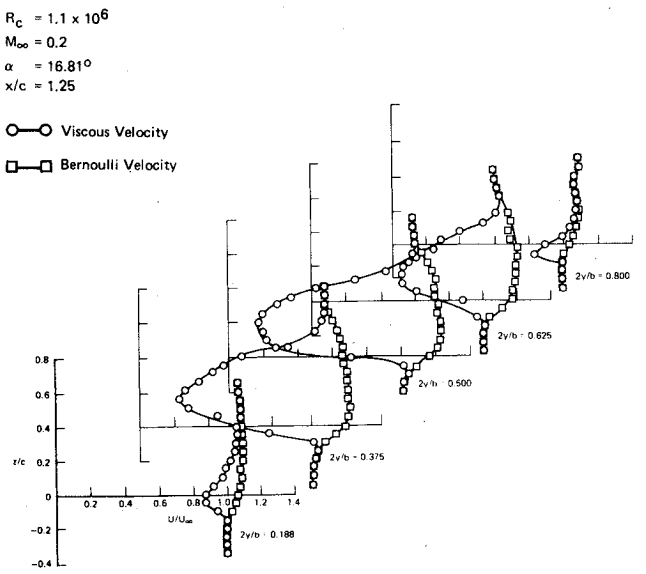

Fig. 12 Representative wake velocity profiles at several spanwise stations for controlled separation wing.

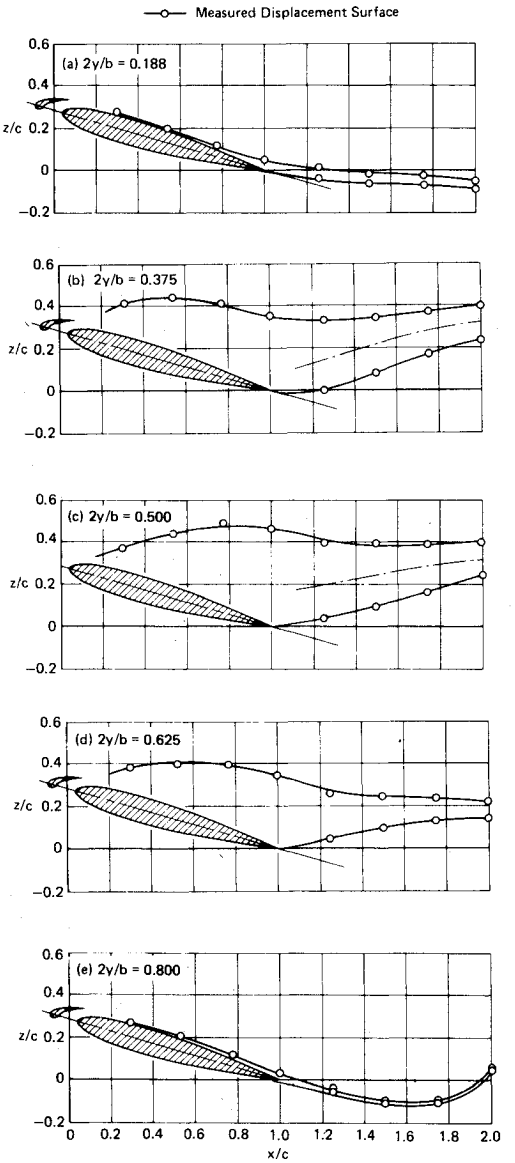

Fig. 13 Equivalent inviscid contour for controlled separation wing ($\alpha = 16.8$ deg, $R_c = 1.1 \times 10^6$).

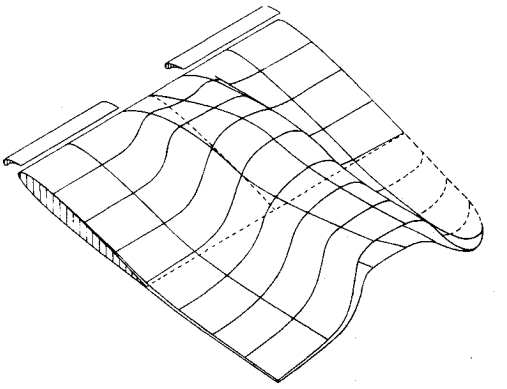

Fig. 14 Isometric view of the equivalent inviscid contour for controlled separation wing ($\alpha = 16.8$ deg, $R_c = 1.1 \times 10^6$).

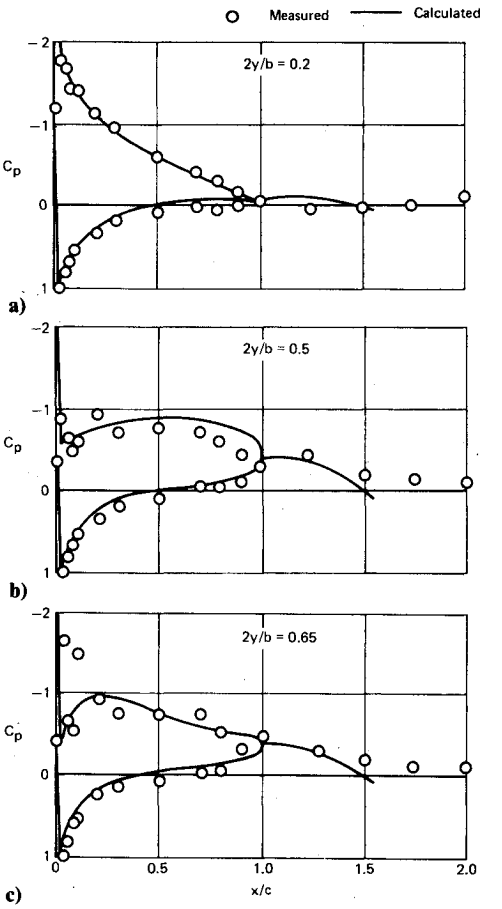

Fig. 15 Pressure coefficients calculated from the measured equivalent wing surface (controlled separation wing, $\alpha = 16.8$ deg, $R_c = 1.1 \times 10^6$).

15a), the centerline of the separated flow region (Fig. 15b), and the outboard edge of the separated flow region (Fig. 15c). It can be seen that the comparison is good.

Conclusions

Detailed measurements have been made of the flowfield around a wing with a controlled midspan region of flow separation at high angles of attack. The bounded flow separation bubble was established by means of inboard and outboard leading-edge slats with an unprotected region between the segments. Flow separation occurred within this unprotected region at angles of attack less than those at which the unslatted wing stalled. The flow did not separate from the regions protected by the slats up to the highest angle of attack tested ($\alpha = 25$ deg).

The boundary between the separated and attached flow regions is characterized by a large circulatory flow on the surface of the model. The circulatory flow is a result of the spanwise pressure gradients induced by the presence of the separation. The separation bubble covered the major portion of these circulating patterns and the region between them. Thus, they can be related to the vorticity within the separation bubble.

For the development of an analytical prediction method, the viscous flow within the separation bubble can be modeled by an equivalent potential flow wing shape. This is analogous to the displacement thickness of a boundary layer. The equivalence was demonstrated by constructing the equivalent wing shape of the controlled separated flow bubble from the flowfield measurements above and aft of the wing. Pressures predicted from calculations of the potential flow around this equivalent wing compared well with those measured on the model surface and in the viscous flow.

References

[1] Kroeger, R.A. and Feistel, T.W., "Reduction of Stall-Spin Entry Tendencies Through Wing Aerodynamic Design," Paper 760481 presented at SAE Business Aircraft Meeting, April 6-9, 1976.

[2] Feistel, T.W., Kroeger, R.A., and Anderson, S.B., "A Method of Localizing Wing Flow Separation at Stall to Alleviate Spin Entry Tendencies," AIAA Paper 78-1476, Aug. 1978.

[3] Gross, L.W., "The Prediction of Two-Dimensional Airfoil Stall Progression," AIAA Paper 78-155, Jan. 1978.

[4] Meznarsic, V.F., Dowgwillo, R.M., and Gross, L.W., "An Investigation of the Flow Characteristics of a Wing Having a Controlled Partial Span Stall," McDonnell Douglas Corp. Rept. MDC A6232, Dec. 1979.

[5] Schollenberger, C.A. and Kotansky, D.R., "A Basic Three-Dimensional Wing/Jet Interaction Experiment," AIAA Paper 75-1219, Oct. 1975.

[6] Gregory, N., Quincey, V.G., O'Reilly, C.L., and Hall, D.J., "Progress Report on Observations of Three-Dimensional Flow Patterns Obtained During Stall Development on Aerofoils, and on the Problem of Measuring Two-Dimensional Characteristics," British ARC CP-1146, 1971.

[7] Alber, E.E., Bacon, J.W., and Masson, B.S., "An Experimental Investigation of Turbulent Transonic Viscous-Inviscid Interactions," AIAA Paper 71-565, June 1971.

[8] Winkelmann, A.E., Barlow, J.B., Saini, J.K., Anderson, J.D. Jr., and Jones, E., "The Effects of Leading Edge Modifications on the Post-Stall Characteristics of Wings," AIAA Paper 80-0199, Jan. 1980.

[9] Winkelmann, A.E. and Barlow, J.B., "Flow Field Model for a Rectangular Planform Wing Beyond Stall," *AIAA Journal*, Vol. 18, Aug. 1980, pp. 1006-1008

[10] Woodward, F.A., "Analysis and Design of Wing-Body Combinations at Subsonic and Supersonic Speeds," *Journal of Aircraft*, Vol. 5, Nov.-Dec. 1968, pp. 528-534

[11] Bristow, D.R., "Computer Program to Solve the Three-Dimensional Mixed Boundary Condition Problem for Subsonic or Supersonic Potential Flow," McDonnell Douglas Corp. Rept. MDC A3190, Dec. 1974.